An Instability in Neutron Stars at Birth

Adam Burrows and Bruce A. Fryxell

Calculations with a two-dimensional hydrodynamic simulation show that a generic Raleigh-Taylor–like instability occurs in the mantles of nascent neutron stars, that it is possibly violent, and that the standard spherically symmetric models of neutron star birth and supernova explosion may be inadequate. Whether this "convective" instability is pivotal to the supernova mechanism, pulsar magnetic fields, or a host of other important issues that attend stellar collapse remains to be seen, but its existence promises to modify all questions concerning this most energetic of astronomical phenomena.

By means of numerical simulations, we have investigated a class of violent hydrodynamic instabilities in nascent neutron stars that may transform our picture of the collapse of the core of a massive star (≥ 8 $M_\odot$, where $M_\odot$ is the solar mass) when it dies and the subsequent supernova explosion. It is not known whether these Raleigh-Taylor–like instabilities, which seem to be generic, are peripheral or central to the supernova explosion mechanism, pulsar magnetic fields, and proper motions, or the synthesis of elements such as uranium and thorium. However, as we here attempt to demonstrate, spherically symmetric models are not adequate to describe the rich set of phenomena that attend one of the most violent events in nature.

At the end of the thermonuclear life of a massive star, its Earth-sized core becomes unstable to implosion. Within 1 s, central densities above nuclear densities are achieved, the matter stiffens, the inner core rebounds, and a shock wave is generated. We focus on only the first 30 ms after core bounce and shock generation and therefore do not address the crucial later phase, lasting a few seconds, during which it is thought that the supernova is launched and the familiar compact neutron star emerges from the clearing debris (*1*). The implications of this later phase remain to be discussed. We believe that the separate consideration we give the initial post-bounce evolution in this article is justified by the rich hydrodynamic behavior we discovered, but caution that much remains to be investigated before the full consequences of aspherical development are understood.

The core of our study is a two-dimensional (2-D) numerical simulation of the early hydrodynamic evolution of a proto-neutron star just after the bounce-shock stalls into an accretion shock. A one-dimensional (1-D) Lagrangian supernova code (*2*) was used to follow the collapse of the unstable core of a 20 $M_\odot$ star (*3*) through core bounce at nuclear densities to shock stagnation. The resulting structure was then mapped onto the 2-D Eulerian hydrodynamics code we developed for this problem and carried for an additional 20 ms. Our 2-D code is a variant of the code constructed by Arnett, Fryxell, and Müller (*4*) who used the piecewise parabolic method (PPM) of Woodward and Colella (*5*). It is Newtonian and has a vectorized nuclear equation-of-state, but no neutrino transfer or neutrino sources and sinks. Full radiative transfer is important for the proper treatment of the supernova problem and must be included in subsequent studies, but its omission should not alter in a qualitative way the purely hydrodynamic results we show here. The calculations were done in cylindrical symmetry with $200(r) \times 100(\theta)$ zones. The region from 50 km to 2000 km was followed even though most of the early action occurs interior to the 300 km radius. The inner boundary and the $\theta = 0°$ and 90° lines were made reflecting.

The supernova problem. Massive stars (≥ 8 $M_\odot$) evolve electron-degenerate cores of iron or Ne-O-Mg that grow to the critical Chandrasekhar mass (~ 1.4 $M_\odot$) and then gravitationally collapse (*6*). Core collapse begins a sequence of events that ends in stellar death, a supernova, and neutron star birth. Occupying the inner few thousand kilometers of a red or blue supergiant, the core at collapse has a central temperature near 0.5 MeV ($\sim 6 \times 10^9$ K), a central density (ρ_c) near 6×10^9 g cm^{-3}, and an entropy per baryon per Boltzmann constant (*s*) near 1.0 (*7*). The latter is a crucial quantity, for its value measures thermodynamic order, its increase signals irreversibility and dissipation, and its slope can drive Raleigh-Taylor–like instabilities in an effective or actual gravitational field. The detailed physics of collapse has been described in many works and is not discussed in this article. However, a few salient points bear mentioning. Collapse proceeds to central densities near and above nuclear densities ($\geq 2.7 \times 10^{14}$ g cm^{-3}) in 0.1 to 1.0 s, during which time the core entropy changes little and the baryons are contained in nuclei. Although there is some electron capture and neutronization during infall, the core becomes opaque to electron-capture neutrinos soon after densities of 10^{11} g cm^{-3} are reached. As a consequence, the lepton number (Y_l, the number of electrons plus electron neutrinos, per baryon) is trapped and frozen (*8*) at values near ~ 0.35. This is far above final neutron star values (~ 0.05) and not too far below those for normal nonhydrogenic terrestrial matter (0.5). The entropy or temperature, the mass density, and the lepton fraction determine all other thermodynamic quantities. At low densities, electron neutrinos are not trapped and the electron fraction (Y_e) substitutes for Y_l as the composition variable in the equation-of-state.

On the above trajectory, collapse would proceed unimpeded to a black hole. The relativistic leptons that dominate the pressure are too soft (adiabatic index, $\gamma \sim 4/3$) to counter gravity. However, upon achieving nuclear densities, the nuclei dissolve into nucleons, which because they are nonrelativistic and repelled by the nuclear force constitute a sufficiently stiff gas ($\gamma > 5/3$) to reverse the infall. The subsonic inner core bounces within tenths of milliseconds and collides with the lower density, supersonic outer core. A shock wave, the bounce shock, is generated at the interface near a radius of 20 km and an interior mass of 0.7 $M_\odot$. The shock wave "entropizes" the material it encounters to peak values between 8 and 10 ($>>1.0$) and has an initial speed near 6×10^9 cm s^{-1} (~ 60 km ms^{-1}). If it continued directly out into the star, it would be the supernova explosion wave. This is the so-called "prompt" scenario for the supernova explosion. However, all complete one-dimensional supernova simulations indicate that this bounce shock stalls within ~ 10 ms between 100 and 300 km and at interior masses near 1.1 $M_\odot$ owing to a fatal combination of nuclear dissociation and copious neutrino radiation when the shock "breaks out" of the neutrinosphere (the "photosphere" or effective radiating surface for neutrinos) (*9*). This saps the shock of its vitality and all post-shock velocities go negative. Crucially, as it weakens the shock leaves behind material of lower and lower entropy. A large entropy spike and a negative entropy gradient are established in the outer core naturally and generically on dynamical times (*10*). Furthermore, a trough in lepton number is established around the neutrinosphere owing to rapid electron capture at shock breakout (*11*).

A. Burrows is in the Departments of Physics and Astronomy, University of Arizona, Tucson, AZ 85721. B. A. Fryxell is at the Goddard Space Flight Center, Greenbelt, MD 20771.

The scenario we have just sketched does not end in a supernova. Nevertheless, astronomical and statistical data imply that a supernova is the outcome of stellar collapse most of the time. That the prompt mechanism aborts is the "supernova problem," and a leading contender for its resolution has been provided by Wilson (*12*). In this long-term or "delayed" mechanism, the neutrinos issuing from the protoneutron star deposit a fraction of their energy via absorption and scattering in the tenuous outer shocked envelope. As the accretion of the rest of the star subsides and the accretion ram pressure at the shock diminishes, the neutrino-heated bubble behind the shock expands and the explosion recommences. Delay times are typically ~1.0 s. A tightly bound neutron star remains after spending its energy in neutrino radiation, a fraction of which is tapped to eject the marginally bound (a few $\times 10^{50}$ ergs) star. In this model, neutrino radiation mediates the transfer of energy from the core to the envelope. However, Wilson needs to enhance his neutrino luminosities by ~20 percent by mixing heat out of the protoneutron star via a doubly diffusive "salt-finger" instability, leptons substituting for salt in this context (*13*). This is suggestive of what may be required for explosion. Bruenn (*14*) has also obtained explosions via an unboosted Wilson-like mechanism. Yet, neither group is achieving explosions of sufficient energy to explain observed supernova, such as SN1987A (1 to 2 $\times$ 10^{51} ergs). Rather, each generates rather anemic explosions ($\leq 4 \times 10^{50}$ ergs) at ~1/4 to 1/3 the required energies.

What is amiss? It could be that the outer "iron" cores are initially much more tenuous than those now calculated (*6*, *15*) and that the bounce shock encounters no appreciable ram pressure or tamping. If this were the case, without tamping even a stalled shock would quickly revive. Such a shock could be aided at the outset by neutrino heating and evolve into a neutrino-driven wind (*10*, *16*). Unfortunately, the residual neutron stars would be too light ($\lesssim 1.2\ M_\odot$). However, it has been suggested (*10*) that there is a natural mechanism for boosting the core luminosities that would drive a vigorous Wilson mechanism: direct hydrodynamic instabilities at the shock-generated entropy spike. The negative entropy gradients referred to earlier are obviously unstable to convective overturn (via the Schwarzschild or Ledoux criteria) (*17*). The unstable region is near the neutrinosphere and might enhance neutrino radiation by direct advective heat transport. Furthermore, as has recently been pointed out (*18*, *19*), core neutrino heating can generate negative entropy gradients in a stalled configuration near the shock and, hence, can drive large-scale convective motions that might be central to the explosion. The inner instability that can boost the driving neutrino flux might couple in interesting ways to the outer instability that can regulate the accretion onto the central star. Whatever the true nature and number of the instabilities in protoneutron stars and however important or peripheral they are to a supernova explosion, they can no longer be ignored. These calculations concerning the entropy-spike instability are presented here mindful of this injunction and in the spirit of initial and very tentative exploration.

Description of the shock-spike instability. The Brünt-Väisälä analysis, which embodies the linear buoyancy theory, yields for the initial growth rate, N,

$$N^2 = g\left(\frac{\partial \ln \rho}{\partial r} - \frac{1}{\gamma}\frac{\partial \ln P}{\partial r}\right) \quad (1)$$

$$= -\frac{g}{\gamma}\frac{\partial \ln P}{\partial s}\bigg|_{\rho,y}\frac{\partial s}{\partial r} \sim -\frac{g}{\gamma C_v}\frac{\partial s}{\partial r}\ \text{(ideal gas)} \quad (2)$$

where γ is the adiabatic index, P is the pressure, g is the effective gravity, r is the radius, C_v is the specific heat at constant volume, and y represents the composition. Equation 2 is based on the assumption that the composition gradients are small, something that we did not assume in the simulations. In the incompressible limit ($\gamma \rightarrow \infty$), Eq. 1 reduces to the standard Raleigh-Taylor instability in which density inversions alone drive overturn and mixing. The Raleigh-Taylor instability is the incompressible limit of compressible convection, which, as Eq. 2 states, is driven by negative entropy gradients. By and large this is the case in the Earth's troposphere and in the convective zones of stars. In the early protoneutron star context that we address here, $|\partial s/\partial r|$ is extreme, ranging from 1.0 to 2.0 units per 10 km. For the initial structure that we used in these calculations, the region that was unstable according to the linear analysis ranged from ~80 km to 110 km ($\Delta r \sim 30$ km) (0.9 $M_\odot$ to 1.0 $M_\odot$ enclosed mass) and involved an entropy drop of ~6 units. Using Eq. 2, we anticipate a growth time ($\tau \sim 3/N$) and maximum flow speed ($V_{max} \sim N\Delta r$) of the overturn of about 3 ms and 2×10^9 cm s^{-1}, respectively. These are just under sound travel and dynamical (approximately free-fall) values and imply that the overturn will be quite violent. However, we caution that these specific results are sensitive to the initial entropy distribution that we employed and, therefore, may not be generic. The energy available to power the overturn motion is the change in the gravitational potential energy under the inversion of the unstable region and is estimated to be approximately 10^{51} ergs. This is indeed approximately $\frac{1}{2}\Delta M V_{max}^2$. So violent is this entropy-spike instability expected to be that one might have thought that it would act as the shock stalls and itself smooth out the gradient that drives it. By only a factor of 2 to 3 in the relevant time scales, this is not the case. The negative gradient imposed dynamically is not smoothed on dynamical times. However, the mapping of the 1-D calculation onto the 2-D grid could have been performed earlier in the calculation (though the precise time does depend upon the magnitude of the seed perturbation). Such subtleties do not seem to effect the qualitative nature of the dynamics and we will ignore them henceforth.

We are presenting our results as a representative set of 2-D color contour plots, a color representing a range of values of a plotted parameter, and, therefore, we eschew the detailed analysis in order to communicate at a glance the qualitative character of the flow. Figures 1 to 4 show 20 ms in the early development of the shock-spike instability. They involve the density (Fig. 1), temperature (Figs. 2 and 3), and the lepton fraction (Fig. 4) every 5 ms after the bounce-shock fails (about 10 ms after bounce). Figure 3 shows the temperature distribution only at the end of the calculation and has velocity vectors superposed. Initially, a random perturbation in the radial and θ velocities, whose maximum magnitude reached 5 percent of the local speed of sound, was applied at each zone. No rotation was imposed. This initial perturbation is well within the range expected as a result of pre-collapse convective motions. Furthermore, the linear regime during which the exact nature of the perturbation is relevant, lasts for at most ~5 ms. As a consequence, the nature and interpretation of the subsequent overturning motions is expected to be roughly independent of the initial perturbation applied.

Shown in Fig. 1 is the density distribution every 5 ms for 20 ms after the shock stalled about 10 ms after bounce. Time increases in the counterclockwise direction from the top right. The vertical and horizontal axes are 250 km long. The colors represent density in reverse rainbow order. High densities are in red at about $\times 10^{11}$ g cm^{-3} and the lowest densities are in deep blue. With the color map chosen, deep blue encompasses all densities below about 10^9 g cm^{-3}. The position of the stalled shock is clearly seen as the line between the dark and light blue regions. The Mach number just exterior to the shock ranges between 3.5 and 3.9, while that just interior to the shock is around 0.2.

The overturn is quite violent, as Fig. 1 demonstrates. Within 10 ms, a well-developed Raleigh-Taylor–like spike and bubble

pattern has developed. About four "mushroom clouds" are visible at this time (top left of Fig. 1). Velocities of 1.5×10^9 cm s^{-1} have been reached and large-scale plumes and penetrating fingers are forming. Furthermore, there is significant overshoot both above and below the initial region of linear instability. At the end of the calculation at 20 ms (bottom right of Fig. 1) the circulation pattern has penetrated all the way to the artificially imposed 50-km boundary and out to a radius of about 160 km, and the eddy size has grown to encompass approximately 100 km on a side. By this time, Mach numbers of 1.0 to 1.5 can be found in the flow, indicating that the entropy-spike drives trans-sonic (near the speed of sound), compressible "convection." The magnitude of the overshoot is important, for the neutrinospheres are penetrated and heat and leptons must be dredged up during at least the first ~50 ms after bounce. This may enhance the neutrino luminosities in just the way necessary to facilitate or speed up the neutrino-mediated long-term mechanism of collapse supernovae. We must emphasize again that we have not here performed the complete radiative transfer calculations necessary to demonstrate the importance or existence of this convective boost. Nevertheless, the qualitative character of these results is very suggestive and encouraging.

The corresponding evolution of the temperature distribution is shown in Fig. 2. High temperatures found predominantly in the interior are rendered in red and range up to 6 MeV, while the low temperatures are in blue and get down to 0.2 MeV. The stalled shock is at the blue-green interface in all four panels. As one might expect, structures similar to those found in Fig. 1 repeat in Fig. 2. Figure 3 depicts the temperature field 20 ms after the shock stalls and contains superposed velocity vectors. Figure 3 is a blown-up version of the fourth quadrant of Fig. 2. At the end of the calculation, the redistribution of entropy has resulted in sinking and compression of the inner mass zones and the slight expansion of the outer mass zones, in just the way anticipated by cruder calculations (*20*). However, the shock wave is only about 10 percent further out in radius than in the corresponding 1-D calculations. These overturning motions in themselves do not result in a supernova. Nevertheless, we expect that combining convection with neutrino energy transfer and electron capture will both accelerate the collapse of the inner mantle and drive the shock to larger radii during the first 50 ms or so after bounce. The early convective boost in the neutrino luminosities may be required to push the shock beyond the so-called "gain radius," exterior to which neutrino heating exceeds neutrino cooling. Hence, entropy-spike convection may be required to enable the long-term mechanism itself (*12*, *13*).

As inner radial slices through the quadrants in Fig. 2 suggest, the early neutrinosphere near 60 km will have hot spots and will flicker on millisecond time scales. This may be nothing more than an intriguing curiosity. However, the evolution of the lepton distribution depicted at the bottom of Fig. 4 may have more profound consequences. What is shown there is the mixing of neutron-rich (red) material from the high density core into the outer shocked mantle. If eventually even 10^{-4} $M_\odot$ of this material is ejected in the explosion, both iron-peak and r-process nucleosynthesis will be radically altered (*21*).

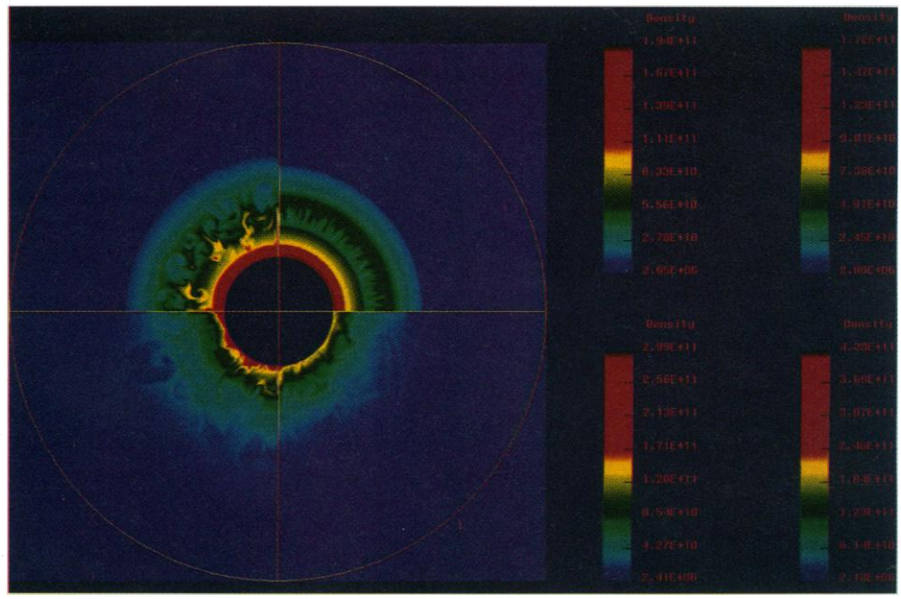

Fig. 1. The density distribution in the simulated protoneutron star 5, 10, 15, and 20 ms after the shock stalls about 10 ms after bounce, in counterclockwise order. The inner boundary of the calculation is at 50 km and both the vertical and horizontal axes are 250 km in length. The position of the shock in each panel is clearly discerned as the color jump from dark blue to light blue. The color bars change slightly from quadrant to quadrant and are in the same counterclockwise order.

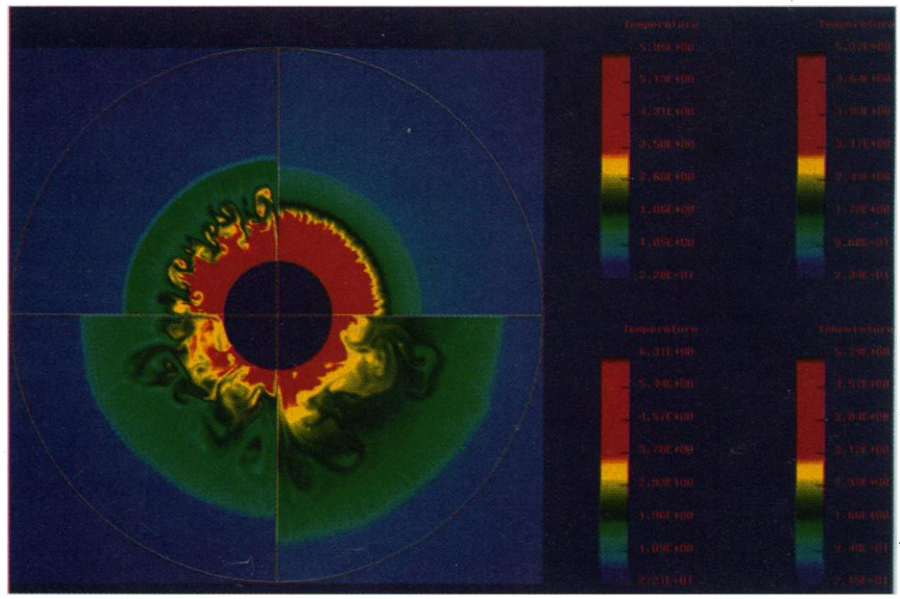

Fig. 2. The temperature distributions of the calculation 5, 10, 15, and 20 ms after shock stagnation, as in Fig. 1. The color bars change slightly from quadrant to quadrant and are in the same counterclockwise order. Red represents regions where the temperature is about 3 to 6 MeV and light blue represents regions where the temperatures are below about 0.8 MeV.

At a minimum, Figs. 1 to 4 demonstrate that protoneutron stars are not spheres. What the violence and extent of the overturn suggest is that the entropy-spike instability cannot be ignored during the first 50 ms after bounce. It may radically alter the early neutrino luminosities that are crucial to the long-term, neutrino-mediated resuscitation of the shock and may even enable it by positioning the shock beyond the gain radius during the early post-bounce evolution. However, it is not yet clear that this macro-convective motion is sustainable. It may be a ~50-ms transient whose echo has faded by the time the supernova is finally launched. Encouragingly, 1-D cooling calculations of protoneutron stars (*14, 22*) that suppress this entropy-driven instability yield steeply negative entropy gradients on the periphery of the protoneutron star during at least the first 500 ms. This implies that convective motions in young neutron star mantles may persist to enhance the driving neutrino emissions during the entire phase for which such emissions are crucial to "re-igniting" the supernova. If this is the case, the doubly diffusive "salt-finger" instabilities deep in the core, posited by Mayle and Wilson (*13*) to provide a needed ~20 percent boost in his neutrino luminosities, may be less important in the supernova explosion mechanism than the entropy-driven instabilities. The resolution of this question awaits more detailed calculations with neutrino transfer.

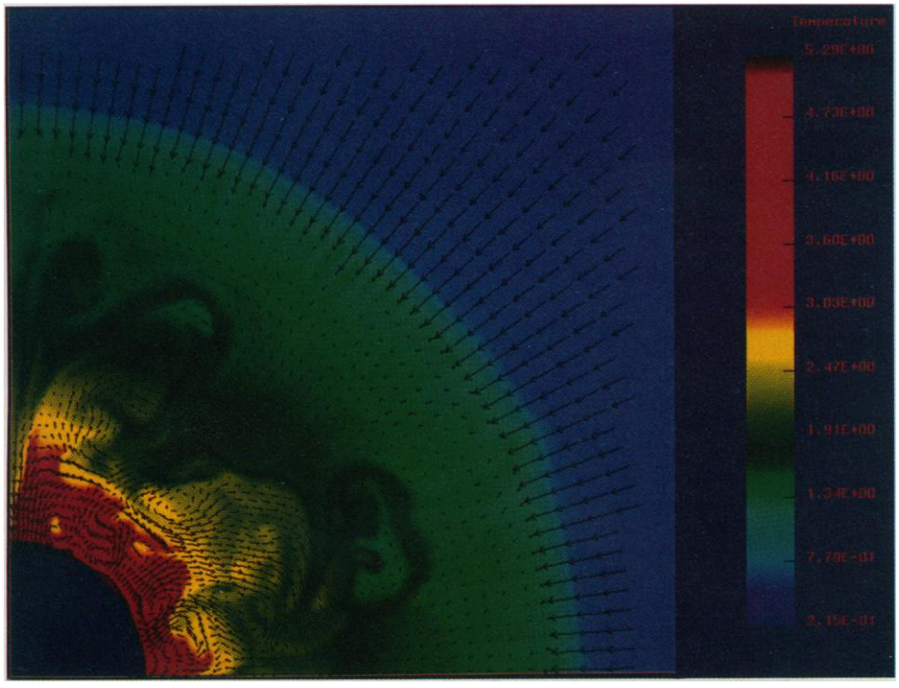

Fig. 3. The temperature distribution at the end of the calculation, 20 ms after shock stagnation. This plot depicts the same data that are found in quadrant four of Fig. 2. Velocity vectors that trace the flow are superposed. The position of the shock is clearly seen to be where there is an abrupt jump in the length of the vectors.

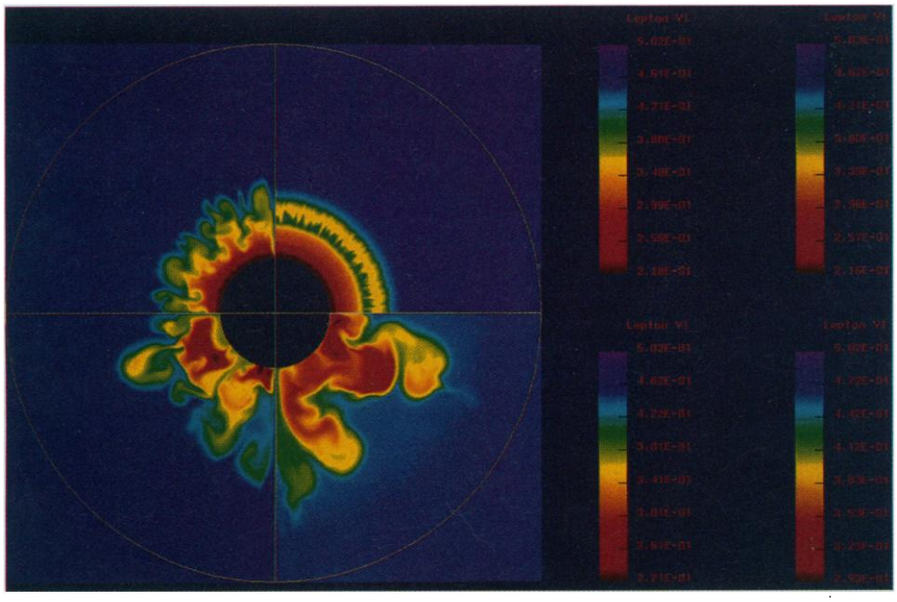

Fig. 4. A composite of lepton fraction distributions that are at 5, 10, 15, and 20 ms after shock stagnation, in counterclockwise order. The color bars change slightly from quadrant to quadrant and are in the same counterclockwise order. Purple represents regions where the entropies are from around 8 to 10 and dark red represents regions where the entropy is below 3. Each quadrant covers the same sections of the star that were cut out in Figs. 1 and 2, at the same times. Red represents low lepton fractions between 0.2 and 0.3 and purple represents lepton fractions near 0.5. The outward mixing of low lepton fraction, neutron-rich material is shown.

Thoughts on the future of supernova theory. We have demonstrated that the mantles of protoneutron stars bounded by stalled bounce shocks are violently unstable to overturn and mixing early in their lives. There is significant penetration beyond the initially unstable region on time scales of a few tens of milliseconds. The instability is trans-sonic and some mass reaches speeds in excess of 10^9 cm s^{-1}. There is a suggestion that the neutrinosphere is breached and that heat and leptons can be dredged up from the entropy spike generically laid down by the bounce shock before it stalls into accretion. The consequent boost in the neutrino luminosities may facilitate, accelerate, or even enable the "re-ignition" of the supernova via the long-term neutrino-driven mechanism. The instability on which we have focused could effect not only supernova energetics and the supernova mechanism, but *r*-process nucleosynthesis, pulsar kicks, supernova neutrino and gravitational radiation signatures, and pulsar magnetic fields. The motions depicted in Figs. 1 to 4 will, at the very least, restructure any seed magnetic field distributions because of the high electrical conductivity of these objects, but even dynamo action is not ruled out (*23*). Furthermore, this inner, early instability could seed with perturbations the outer, later instability highlighted in (*19*).

These calculations and those of Herant *et al.* (*19*) introduce a new level of complexity into supernova modeling that has been forced upon us both by the existence of fascinating instabilities and by the persistence of the supernova problem. Multidimensional simulations seem to be the future of the field. What has occurred is not

a "paradigm shift," but a gradual convergence of technique and need. The many approximations and compromises of these 2-D simulations will gradually be eliminated and what promises to emerge is a rich and detailed picture of one of the most dramatic natural events.

REFERENCES AND NOTES

1. A. Burrows, *Annu. Rev. Nucl. Part. Sci.* **40**, 181 (1990).
2. _____ and J. M. Lattimer, *Astrophys. J.* **299**, L19 (1985).
3. T. A. Weaver, S. E. Woosley, G. E. Fuller, in *Numerical Astrophysics*, J. M. Centrella, J. M. LeBlanc, R. L. Bowers, Eds. (Jones and Bartlett, Boston, 1985), p. 374.
4. W. D. Arnett, B. A. Fryxell, E. Müller, *Astrophys. J.* **341**, L63 (1989).
5. P. Woodward and P. Colella, *J. Comp. Phys.* **54**, 115 (1984).
6. S. E. Woosley and T. A. Weaver, *Annu. Rev. Astron. Astrophys.* **24**, 205 (1986).
7. A. Burrows, *Phys. Today* **40**, 28 (1987).
8. T. J. Mazurek, *Nature* **252**, 287 (1974); K. Sato, *Prog. Theor. Phys.* **54**, 1325 (1975); W. D. Arnett, *Astrophys. J.* **218**, 815 (1977); W. Hillebrandt and E. Muller, *Astron. Astrophys.* **103**, 147 (1981).
9. T. J. Mazurek, *Astrophys. J.* **259**, L43 (1982); S. W. Bruenn, *Astrophys. J. Suppl.* **58**, 771 (1985).
10. A. Burrows, *Astrophys. J.* **318**, L57 (1987).
11. _____ and T. J. Mazurek, *ibid.* **259**, 330 (1982).
12. J. R. Wilson, in *Numerical Astrophysics*, J. Centrella, J. LeBlanc, R. L. Bowers, Eds. (Jones and Bartlett, Boston, 1985), p. 422.
13. R. Mayle and J. R. Wilson, *Phys. Rep.* **163**, 63 (1988).
14. S. W. Bruenn, in preparation.
15. K. Nomoto, T. Shigeyama, M. Hashimoto, in *Proceedings of the IAU Colloquium 108 on Atmospheric Diagnostics of Stellar Evolution: Chemical Peculiarity, Mass Loss and Explosion*, K. Nomoto, Ed. (Springer-Verlag, Berlin, 1987), p. 319.
16. S. E. Woosley and E. Baron, *Astrophys. J.* **391**, 228 (1992).
17. J. P. Cox and R. T. Guili, *Principles of Stellar Structure* (Bordon and Breach), New York, 1968).
18. H. A. Bethe, *Rev. Mod. Phys.* **62**, 801 (1990).
19. M. Herant, W. Benz, S. A. Colgate, *Astrophys. J.* **395**, 642 (1992).
20. A. Burrows and J. M. Lattimer, *Phys. Rep.* **163**, 51 (1988); H. A. Bethe, G. E. Brown, J. Cooperstein, *Astrophys. J.* **322**, 201 (1987).
21. S. E. Woosley and R. Hoffman, *Astrophys. J.* **395**, 202 (1992); B. S. Meyer *et al.*, *ibid.*, in press.
22. A. Burrows and J. M. Lattimer, *ibid.* **307**, 178 (1986).
23. R. Duncan and C. Thompson, *ibid.*, in press; C. Thompson and R. Duncan, *ibid.*, in press.

24. We thank NSF and NASA for support under grants AST89-14346 and NAGW-2145, respectively, and acknowledge the hospitality of the Aspen Center for Physics, where some of this manuscript was generated. Conversations with D. Arnett, T. Weaver, S. Woosley, and W. Benz materially improved the paper. These calculations were performed at the National Center for Supercomputer Applications (NCSA) at Urbana, IL, and the graphics were created on a Silicon Graphics 4D/35 workstation.

24 July 1992; accepted 15 September 1992

Atomic Structure of the DNA Repair [4Fe-4S] Enzyme Endonuclease III

Che-Fu Kuo, Duncan E. McRee, Cindy L. Fisher, Suzanne F. O'Handley, Richard P. Cunningham, John A. Tainer*

The crystal structure of the DNA repair enzyme endonuclease III, which recognizes and cleaves DNA at damaged bases, has been solved to 2.0 angstrom resolution with an *R* factor of 0.185. This iron-sulfur [4Fe-4S] enzyme is elongated and bilobal with a deep cleft separating two similarly sized domains: a novel, sequence-continuous, six-helix domain (residues 22 to 132) and a Greek-key, four-helix domain formed by the amino-terminal and three carboxyl-terminal helices (residues 1 to 21 and 133 to 211) together with the [4Fe-4S] cluster. The cluster is bound entirely within the carboxyl-terminal loop with a ligation pattern (Cys-X_6-Cys-X_2-Cys-X_5-Cys) distinct from all other known [4Fe-4S] proteins. Sequence conservation and the positive electrostatic potential of conserved regions identify a surface suitable for binding duplex B-DNA across the long axis of the enzyme, matching a 46 angstrom length of protected DNA. The primary role of the [4Fe-4S] cluster appears to involve positioning conserved basic residues for interaction with the DNA phosphate backbone. The crystallographically identified inhibitor binding region, which recognizes the damaged base thymine glycol, is a seven-residue β-hairpin (residues 113 to 119). Location and side chain orientation at the base of the inhibitor binding site implicate Glu^{112} in the *N*-glycosylase mechanism and Lys^{120} in the β-elimination mechanism. Overall, the structure reveals an unusual fold and a new biological function for [4Fe-4S] clusters and provides a structural basis for studying recognition of damaged DNA and the *N*-glycosylase and apurinic/apyrimidinic–lyase mechanisms.

Damage inflicted on DNA by active oxygen species has been implicated in many degenerative processes, including cancer and aging (*1*). All cells have an arsenal of highly efficient DNA repair mechanisms to cope with the multitude of lesions formed. The base excision repair mechanism is initiated by the sequential action of ubiquitous DNA *N*-glycosylases and AP endonucleases, suggesting that all organisms make use of this mode of DNA repair (*2*). Endonuclease III of *Escherichia coli* acts both as a DNA *N*-glycosylase, removing oxidized pyrimidines from DNA, and an apurinic/apyrimidinic (AP) lyase, introducing a single-strand nick at the AP site from which the damaged base was removed (*3*). Investigation of the *E. coli* enzyme has the advantage that results from the extensively studied bacterial systems for protection and repair responses to oxidative stress are often applicable to more complex and less defined systems, including human cells (*4*). Bacteria (*5*, *6*), yeast (*7*), and bovine and human cells (*8*) share a conserved class of enzymes with the same substrate specificity for damaged DNA cleavage, similar molecular weights, and no requirement for divalent cations. Because endonuclease III is the prototype for this conserved class of enzymes, studies of the protein have broad implications in understanding DNA repair and, potentially, carcinogenesis and aging in higher organisms. Endonuclease V, whose structure was recently reported (*9*), is a different enzyme of distinct structure but related function that is found in phages and is without known homologs in higher organisms.

Cloning and overexpression of the *nth* gene has allowed large-scale purification and biochemical characterization of endonuclease III (*5*, *10*). Surprisingly, the protein, unlike any of the other well-characterized DNA repair enzymes, contains an iron-sulfur [4Fe-4S] cluster. Sequence similarity suggests that the recently sequenced *mutY* gene codes for an adenine glycosylase that also contains an Fe-S cluster (*11*) and that endonuclease III is a representative of a new class of Fe-S proteins. The three-dimensional (3-D) structure of endonuclease III provides detailed information to guide biochemical investigations into the enzyme's recognition of damaged DNA, the biological function of the [4Fe-4S] cluster, and the mechanisms for the *N*-glycosylase and AP lyase activities. The combined structural and biochemical results show that endonuclease III contains novel structural motifs for the recognition and repair of damaged DNA previously unidentified in a

C.-F. Kuo, D. E. McRee, C. L. Fisher, and J. A. Tainer are at the Department of Molecular Biology, The Scripps Research Institute, La Jolla, CA 92037. S. F. O'Handley and R. P. Cunningham are at the Center for Biochemistry and Biophysics, Department of Biological Sciences, State University of New York at Albany, Albany, NY 12222.

*To whom correspondence should be addressed.